

# Identification of epitaxial $Y_2O_3$ inclusions in sputtered $YBa_2Cu_3O_7$ films: Impact on film growth

A. Catana, R. F. Broom, J. G. Bednorz, J. Mannhart, and D. G. Schlom  
*IBM Research Division, Zurich Research Laboratory, 8803 Rüschlikon, Switzerland*

(Received 7 November 1991; accepted for publication 10 December 1991)

$Y_2O_3$  inclusions with typical sizes between 100 and 300 nm<sup>3</sup>, densely distributed ( $10^{16}$  cm<sup>-3</sup>) in sputtered  $YBa_2Cu_3O_7$  (YBCO) films on  $SrTiO_3$  substrates, have been identified by high-resolution electron microscopy. The precipitates exhibit either cuboid or needlelike shapes and grow epitaxially within and on top of YBCO. The dominant orientation relationship corresponds to a situation where the two-dimensional lattices are nearly coincident in the interfacial (001) plane. These precipitates may contribute to the generation of screw and edge dislocations. In addition, they provide a large number of potential pinning sites for magnetic flux lines, which may contribute to the observed high critical current densities.

Knowledge about second phases that are incorporated in nonstoichiometric  $YBa_2Cu_3O_7$  (YBCO) thin films not only relates to the compositional phase diagram, but should also contribute to the understanding of the film structure and growth mechanism. The relation between impurity phases and film morphology has been revealed by scanning electron microscopy analysis of samples with various compositions,<sup>1,2</sup> in which results showed that decreasing the Cu/Y or Ba/Y ratios increases the surface roughness, whereas increasing the Cu content leads to the formation of small CuO deposits on the surface.<sup>3</sup> Additionally, the formation of second phase inclusions may strongly influence the growth mechanism. Indeed, sputtered films with screw dislocations also have a high density of second phase precipitates.<sup>4</sup> Such inclusions may act as flux pinning sites, raising the critical current density.<sup>5</sup> It has recently been reported that Cu- and Y-rich YBCO films grown by electron beam co-evaporation display a large number of  $CuYO_2$  precipitates with preferential orientations,<sup>6</sup> whereas laser ablated films showed grains belonging to several phases, including  $Y_2O_3$ .<sup>7</sup>

In this letter we identify  $Y_2O_3$  precipitates within and on top of sputtered YBCO films, determine their epitaxial relationships and discuss the impact of these inclusions on the final film structure and properties.

The YBCO films were grown by dc hollow cathode magnetron sputtering on nominally (100) oriented  $SrTiO_3$  substrates at temperatures of about 750 °C and growth rates between 0.05 and 0.1 nm/s. The sputtering pressure was 650 mTorr (Ar:O<sub>2</sub> = 2:1), the plasma discharge 155–175 V and 260–450 mA, and after growth the films were cooled down in about 0.5 bar O<sub>2</sub>. Electrical transport measurements showed  $T_c$  values of 87–89 K. Recent surface studies of these films by scanning tunneling microscopy have shown  $10^8$ – $10^9$  screw dislocations per cm<sup>2</sup> which are thought to be correlated with the high critical current densities (up to  $7 \times 10^7$  A/cm<sup>2</sup> at 4.2 K) that were measured.<sup>8,9</sup>

TEM samples were prepared for both planar and cross-sectional views by standard mechanical polishing and ion milling with liquid nitrogen cooling. The observations were performed on a JEOL JEM-2010 operating at 200 kV.

X-ray diffraction shows three peaks corresponding to interplanar spacings of 0.307, 0.264, and 0.132 nm in addition to the characteristic YBCO-001 reflections. This suggests the presence of one or more impurity phases with preferential orientations. From the relative intensities of the extra diffraction peaks it is clear that the dominant orientation of the impurities is with the planes at 0.264 nm parallel to the (001) YBCO planes. The phase that fits the x-ray diffraction data best is  $Y_2O_3$ , in which case the three additional peaks would be associated with the 222, 004, and 008 reflections, respectively. Impurity peaks at 0.307, 0.264, and 0.187 nm have also been observed by Matijasevic *et al.* on Cu- and Y-rich, *e* beam co-evaporated YBCO films.<sup>3</sup> In their study, the first peak was assigned to  $CuYO_2$ , whereas the latter ones remained unassigned. Since they can all be indexed as  $Y_2O_3$  (222, 004, and 440), it is possible that in their films  $Y_2O_3$  precipitates coexist with  $CuYO_2$ .

For an unambiguous structural identification, we used high-resolution electron microscopy (HREM). The planar-view image in Fig. 1 shows a large number of precipitates with sizes between 20 and 50 nm<sup>2</sup>, densely distributed ( $10^{11}$ /cm<sup>2</sup>) within the film. The inclusions display a square lattice rotated by 45° around the [001] YBCO axis, as shown in Fig. 2. The corresponding diffraction pattern (inset in Fig. 2) shows weak spots at about 1/2 (110) YBCO superimposed on the characteristic [001] YBCO pattern. From the fourfold symmetry of the diffraction pattern and lattice image, we conclude that the structure of the precipitates is either cubic or tetragonal.  $Y_2O_3$  is cubic ( $a = 1.06$  nm) and belongs to the space group Ia3. The unit cell contains 16 molecules, with Y in similar positions as Ca in  $CaF_2$ . However, each metallic atom in  $Y_2O_3$  has four oxygen atoms as nearest neighbors. Indexing of the diffraction pattern is consistent with the inclusions being  $Y_2O_3$ . The weak reflections in Fig. 2 correspond to (200)  $Y_2O_3$  spacings, whereas the (400) spots overlap the (110) YBCO reflections. The epitaxial orientation relationship between the  $Y_2O_3$  precipitates and the YBCO film observed in planar views is (001)  $Y_2O_3$  || (001) YBCO and [110]  $Y_2O_3$  || [100] YBCO. This result was confirmed by cross-sectional observations as in Fig. 3, which shows a

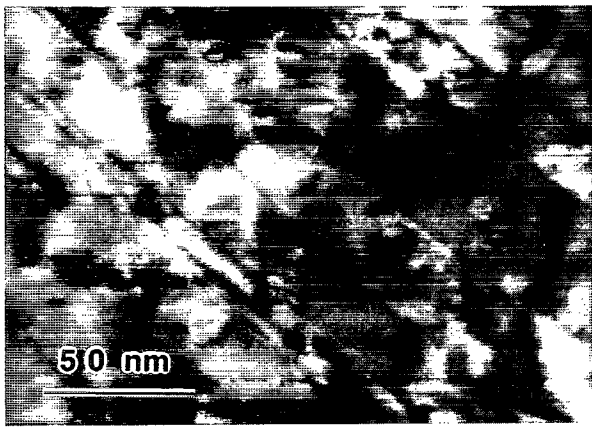


FIG. 1. TEM planar-view of YBCO twins and  $Y_2O_3$  precipitates.

$Y_2O_3$  inclusion projected along  $[110] Y_2O_3 \parallel [100] YBCO \parallel [100] SrTiO_3$  and the calculated image that best matches the experimental image (inset Fig. 3).

From both planar and cross-sectional observations we deduce that the precipitates have typical sizes between 100 and 300 nm<sup>3</sup> and a density of 10<sup>16</sup>/cm<sup>3</sup>.

The presence of  $Y_2O_3$  in YBCO samples is unexpected since no tie line exists between them in the equilibrium phase diagram, even at low oxygen pressures.<sup>10</sup> The existence of  $Y_2O_3$  in films may thus be due to the kinetic hindrance of the nucleation and growth of the expected  $Y_2BaCuO_5$  phase or to lower interfacial energies between YBCO and  $Y_2O_3$ . Considering the highly oriented growth of  $Y_2O_3$ , this latter explanation appears more likely.

The formation of epitaxial  $Y_2O_3$  precipitates is a minor obstacle for the epitaxial overgrowth of YBCO. The overgrown YBCO planes appear distorted with respect to regions in which the growth has not been affected by inclusions, as can be seen by looking at Fig. 3 at a grazing angle. These features can be explained on the basis of lattice-matching arguments. Since the boundaries between precipitates and matrix form at temperatures above 600 °C, at which YBCO is tetragonal, we consider the matching between two square lattices in the (001) interfacial plane: the lattice constants are 1.06 nm for  $Y_2O_3$  and 0.387 nm for YBCO. Lattice mismatch is defined here as the mismatch between supercells obtained by linear combination of the basis vectors of the primitive cells of each crystal. For the observed mutual orientation, the nearly coincident supercells are defined by  $[100] Y_2O_3 \parallel [220] YBCO$  and  $[010] Y_2O_3 \parallel [220] YBCO$  and the resulting mismatch is 3.1%. No other mutual orientations can lead to a higher density of nearly coincident sites in this interfacial plane, which indicates that the observed epitaxy corresponds to a minimum of the interfacial energy. Along the  $[001]$  axis, however, the matching is poor (9.8%) resulting in distorted overgrowth, in agreement with experimental observations as seen in Fig. 3.

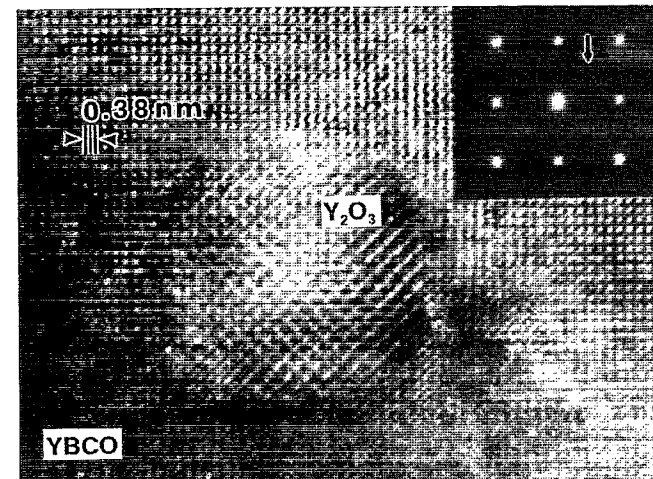


FIG. 2. Lattice image of a  $Y_2O_3$  precipitate and corresponding diffraction pattern (the arrow indicates a 100  $Y_2O_3$  reflection).

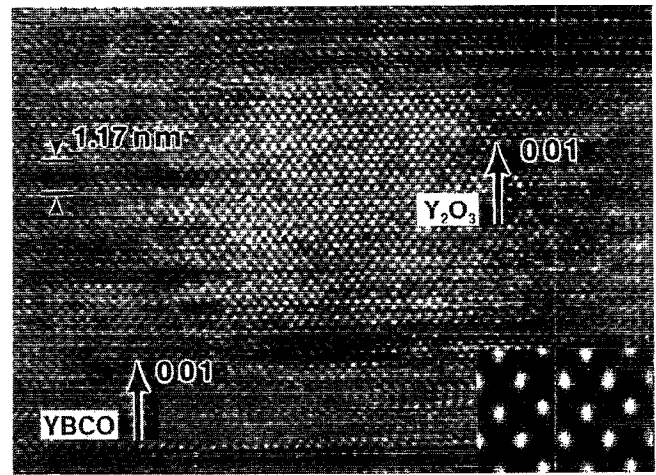


FIG. 3. Cross-sectional micrograph of  $Y_2O_3$  inclusion with (001) planes parallel to the (001) YBCO planes. The inset shows the calculated image along  $[110] Y_2O_3$ ; the microscope parameters are: spherical aberration coefficient = 0.5 mm, spread of focus = 8 nm, beam semi-convergence = 0.8 mrad, defocus = 36 nm; sample thickness = 6 nm.

Some  $Y_2O_3$  inclusions have (110) planes parallel to the (001) YBCO planes; they are different from those satisfying the dominant orientation, in that they are needle shaped with the longitudinal axis parallel to the substrate normal (see Fig. 4). The occurrence of two types of precipitates with distinct epitaxial relations indicates that orientation and shape are correlated.

Precipitates with (111) planes parallel to the (001) YBCO planes are rarely observed, which is consistent with the low intensity of the corresponding diffraction peak with respect to the dominant (004) peak. Although (222) are the closest-packed planes in the  $Y_2O_3$  structure (maximum diffracted intensity), the matching conditions imposed by the surrounding matrix are unfavorable for epitaxial growth with  $(111) Y_2O_3 \parallel (001) YBCO$ .

All inclusion types affect the propagation of a planar growth front; their incorporation introduces strain and defects, such as stacking faults, dislocations, and twin boundaries. For example, when an advancing YBCO growth front encounters a precipitate, the growth front may split

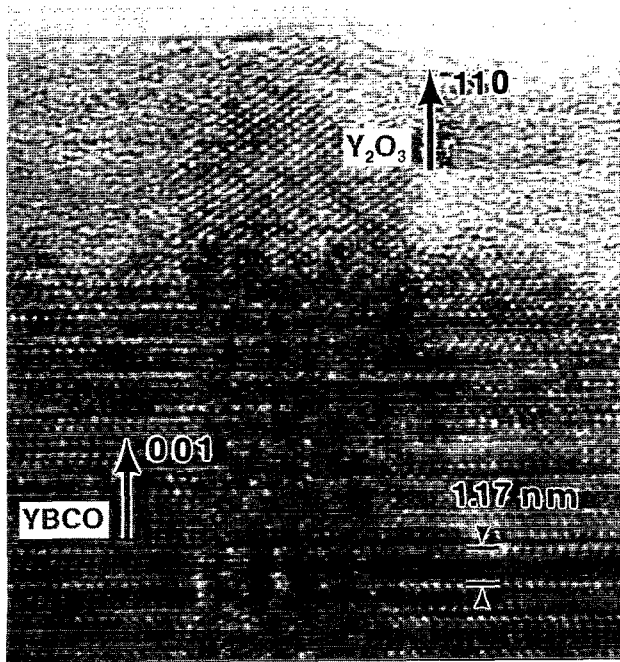


FIG. 4. Needlelike  $Y_2O_3$  inclusion with  $(110) Y_2O_3 \parallel (001) YBCO$ . The inclusion extends about 35 nm into the film.

into two growth fronts advancing around either side of the precipitate. When several growth fronts recombine on the same plane, edge dislocations and translation boundaries may be generated. Such defects have been observed by Streiffer *et al.* in ultrathin YBCO films (1.2–12 nm) deposited onto MgO substrates.<sup>11</sup> The formation of these defects is ascribed to regions of rotational misalignment stemming from the intersection of growing islands. A similar process may also apply to our films, in which case  $Y_2O_3$  precipitates are the origin of rotational misalignments and strains. Growth fronts that are offset from each other may generate a screw dislocation when they later recombine. Such a mechanism has been proposed to explain the formation of growth spirals in mica.<sup>12</sup> It is likely that it also applies to YBCO films, which would explain the high density of screw dislocations that has been observed.<sup>4</sup>

In summary, small  $Y_2O_3$  inclusions in sputtered YBCO films on  $SrTiO_3$  substrates have been identified. They are characterized by either cuboid or needlelike shapes and grow epitaxially within and on top of the YBCO films with two orientations related by a  $90^\circ$  rotation around the common  $[110] Y_2O_3$  and  $[100] YBCO$  axes. In the dominant case, the  $(001) Y_2O_3$  planes are parallel to the  $(001) YBCO$  planes;  $(001) Y_2O_3$  planes parallel to  $(100) YBCO$  planes are also observed for precipitates with distinctly different morphology, indicating that the orientation and shape of the inclusions are correlated. The growth of precipitates satisfying the dominant orientation relation is favorably influenced by the low two-dimensional lattice mismatch in the interfacial  $(001)$  plane. These inclusions and in particular the boundaries and defects that are created affect the further overgrowth of the film. The precipitates lead to strained and misaligned regions, which in turn promote the formation of edge and screw dislocations, twist and translation boundaries. Additionally, they may act as pinning centers and hence influence the critical current density.

It is a pleasure to acknowledge K. A. Müller and J. P. Locquet for stimulating discussions.

- <sup>1</sup>J. A. Edwards, N. G. Chew, S. W. Goodyear, S. E. Blenkinsop, and R. G. Humphries, *J. Less-Common Metals* **164**, 414 (1990).
- <sup>2</sup>J. Zhao, C. S. Chern, Y. Q. Li, P. Norris, B. Gallois, B. Kear, X. D. Wu, and R. E. Münchhausen, *Appl. Phys. Lett.* **58**, 2839 (1991).
- <sup>3</sup>V. Matijasevic, P. Rosenthal, K. Shinohara, A. F. Marshall, R. H. Hammond, and M. R. Beasley, *J. Mater. Res.* **6**, 682 (1991).
- <sup>4</sup>D. G. Schlom, D. Anselmetti, J. G. Bednorz, R. Broom, A. Catana, T. Frey, Ch. Gerber, H. J. Güntherrodt, H. P. Lang, J. Manhart, and K. A. Müller, *Z. Phys. B* (in press).
- <sup>5</sup>M. Murakami, S. Gotoh, N. Koshizuka, S. Tanaka, T. Matsushita, S. Kambe, and K. Kitazawa, *Cryogenics* **30**, 390 (1990).
- <sup>6</sup>A. F. Marshall, V. Matijasevic, P. Rosenthal, K. Shinohara, R. H. Hammond, and M. R. Beasley, *Appl. Phys. Lett.* **57**, 1158 (1990).
- <sup>7</sup>O. Eibl and B. Roas, *J. Mater. Res.* **5**, 2620 (1990).
- <sup>8</sup>Ch. Gerber, D. Anselmetti, J. G. Bednorz, J. Manhart, and D. G. Schlom, *Nature* **350**, 279 (1991).
- <sup>9</sup>J. Manhart, D. Anselmetti, J. G. Bednorz, A. Catana, Ch. Gerber, K. A. Müller, and D. G. Schlom, *Z. Phys. B* (in press).
- <sup>10</sup>R. Beyers and B. T. Ahn, *Ann. Rev. Mater. Sci.* **21**, 335 (1991).
- <sup>11</sup>S. K. Streiffer, B. M. Lairson, C. B. Eom, B. M. Clemens, J. C. Bravman, and T. H. Geballe, *Phys. Rev. B* **43**, 13 007 (1991).
- <sup>12</sup>A. Baronne, *J. Cryst. Growth* **19**, 193 (1973).

Applied Physics Letters is copyrighted by AIP Publishing LLC (AIP). Reuse of AIP content is subject to the terms at: <http://scitation.aip.org/termsconditions>. For more information, see <http://publishing.aip.org/authors/rights-and-permissions>.